

**T.C.**

**DİCLE UNIVERSITY**

**INSTITUTE OF NATURAL AND APPLIED SCIENCES**

**TUNING OXYGEN SENSITIVITY OF RUTHENIUM COMPLEX  
EXPLOITING SILVER NANOPARTICLES**

**Osman ÖZTÜRK**

**MASTER THESIS**

**DEPARTMENT OF CHEMISTRY**

**DİYARBAKIR**

**December, 2014**

DICLE UNIVERSITY  
INSTITUTE OF NATURAL AND APPLIED SCIENCES  
DİYARBAKIR

We have read the thesis entitled “**Tuning Oxygen Sensitivity of Ruthenium Complex Exploiting Silver Nanoparticles**” completed by **Osman ÖZTÜRK** under supervision of **Prof. Dr. Hamdi TEMEL**, and we certify that in our opinion it is fully adequate, in scope and in quality, as a thesis for the degree of Master.

Thesis Committee Members

President : Prof. Dr. Hamdi TEMEL (Supervisor)

Member : Prof. Dr. Berrin ZİYADANOĞULLARI

Member : Yrd. Doç. Dr. Sevgi İRTEGÜN

Date of Thesis Defense Presentation: 31/12/2014

I certify the accuracy of the above information.

.../...../.....

Doç. Dr. Mehmet YILDIRIM

Director  
Institute of Natural and Applied Sciences

## ACKNOWLEDGMENTS

I would like to express my sincere gratitude to my supervisor Prof. Dr. Hamdi TEMEL for providing the fascinating subject, for his valuable support during this thesis and for the great working conditions at our laboratory.

Who lent their help during my experimental work and my thesis work, Prof. Dr. Kadriye ERTEKİN, Prof. Dr. Elif SUBAŞI and Dr. Salih PAŞA

Finally, I would like to thank to my mother, my father and especially to my wife Hasibe ÖZTÜRK, for their tolerant attitude to my working effort during the elaboration of this dissertation and for their incessant support and understanding during all the years of my studies.

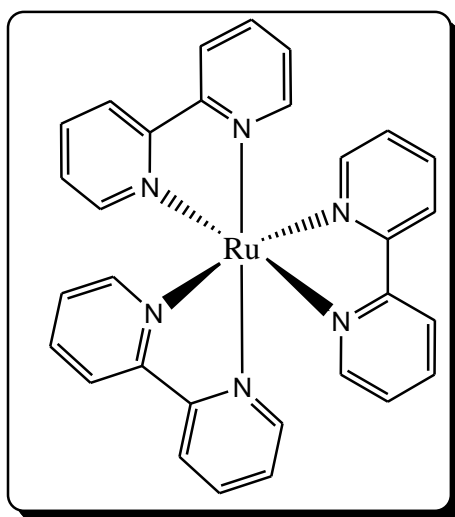
Osman ÖZTÜRK

	<b>PAGE</b>
<b>CONTENTS</b>	
<b>ACKNOWLEDGMENTS</b> .....	<b>I</b>
<b>CONTENTS</b> .....	<b>II</b>
<b>ABSTRACT</b> .....	<b>III</b>
<b>ÖZET</b> .....	<b>IV</b>
<b>LIST OF FIGURES</b> .....	<b>V</b>
<b>ABBREVIATIONS AND SYMBOLS</b> .....	<b>VI</b>
<b>1. INTRODUCTION</b> .....	<b>1</b>
<b>2. MATERIAL AND METHOD</b> .....	<b>5</b>
<b>2.1. Materials</b> .....	<b>5</b>
<b>2.2. Instrumentation</b> .....	<b>5</b>
<b>2.2.1. Electrospinning</b> .....	<b>6</b>
<b>2.2.1.1. Theory of Electrospinning</b> .....	<b>6</b>
<b>2.2.1.2. Parameters of Electrospinning Process</b> .....	<b>8</b>
<b>2.2.1.3. Electrospun Nanofibrous Membranes for Sensors Design</b> .....	<b>8</b>
<b>2.2.1.4. Electrospinning Apparatus</b> .....	<b>9</b>
<b>2.2.1.5. Principles of Optical Chemical Sensors</b> .....	<b>9</b>
<b>2.2.1.6. Classification of Optical Chemical Sensors</b> .....	<b>10</b>
<b>2.3. Gas sensing studies</b> .....	<b>12</b>
<b>2.4. Preparation of silver nanoparticles</b> .....	<b>13</b>
<b>2.5. Preparation of electrospun nanofibers</b> .....	<b>16</b>
<b>3. RESULTS AND DISCUSSION</b> .....	<b>17</b>
<b>3.1. Structural aspect of the sensing materials</b> .....	<b>17</b>
<b>3.2. Fluorescence based measurements</b> .....	<b>19</b>
<b>3.3. Oxygen sensing studies</b> .....	<b>20</b>
<b>3.3.1. Response time and regeneration related sensor dynamics</b> .....	<b>27</b>
<b>4. CONCLUSION</b> .....	<b>29</b>
<b>5. REFERENCES</b> .....	<b>31</b>
<b>RESUME</b> .....	<b>35</b>

## ABSTRACT

### TUNING OXYGEN SENSITIVITY OF RUTHENIUM COMPLEX EXPLOITING SILVER NANOPARTICLES

In this study, we utilized silver nanoparticles (AgNPs) along with ionic liquids as additives for fabrication of polymeric oxygen sensitive fibers. Plasticized polymethyl methacrylate and ethyl cellulose (EC) were used as matrix materials. Fibers and porous films were produced by electrospinning technique. Oxygen induced spectral response of the fluorescent tris(2,2'-bipyridyl) ruthenium(II) chloride ( $\text{Ru}(\text{bipy})_3^{2+}$ ) was followed as the analytical signal. Utilization of silver nanoparticles in electrospun polymeric fibers for oxygen sensing purposes resulted with many advantages such as tuned sensitivity, linear calibration plot for larger concentration ranges, increased surface area and enhancement in all sensor dynamics. Linearity of the calibration plot for the offered composition was superior with respect to the previously reported ones. When stored at the ambient air of the laboratory there was no significant drift in intensity after 12 months. Our sensitivity and stability tests are still in progress.

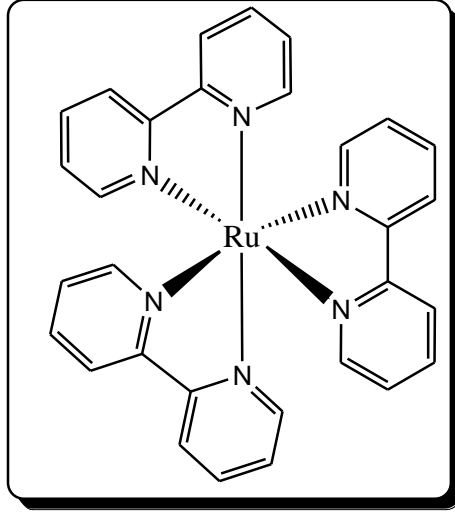


**Tris(2,2'-bipyridyl) dichloro ruthenium(II)**

## ÖZET

### GÜMÜŞ NANOPARTİKÜLLERİ İLAVE EDİLMİŞ RUTENYUM BİLEŞİĞİNİN AYARLANABİLİR OKSİJEN HASSASİYETİ

Bu çalışmada, oksijene karşı duyarlı bir polimer üretimi için katkı maddesi olarak iyonik sıvılar ile birlikte gümüş nanoparçacıkları (AgNPs) kullanılmıştır. Polimerleştirici olarak plastikleştirilmiş polimetil metakrilat ve etil selüloz matris malzemesi olarak kullanılmıştır. Fiber ve gözenekli filmler elektro-eğirme yöntemiyle elde edilmiştir. Floresan özellikli tris(2,2'-bipridil) rutenyum(II) klorür ( $\text{Ru}(\text{bipy})_3^{2+}$ )'nin oksijenden kaynaklı spektral tepkileri analitik sinyaller olarak izlendi. Bileşim için önerilen kalibrasyon eğrisinin lineer özelliği daha önce rapor edilenlerden daha iyi çıkmıştır. Laboratuvar koşullarında depolanarak 12 ay boyunca yapılan ölçümlerde belirgin bir şiddet değişimi olmamıştır. Bu duyarlılık ve kararlılık testleri devam etmektedir.



**Tris(2,2'-bipiridil) dikloro rutenyum(II)**

## LIST OF FIGURES

<u>Figure No</u>		<u>Page</u>
<b>Fig. 1</b>	Tris(2,2'-bipyridyl)dichloro ruthenium(II)	2
<b>Fig. 2.1</b>	Poly(methyl methacrylate)	5
<b>Fig. 2.2</b>	Ethyl Cellulose	5
<b>Fig. 2.3</b>	The most frequently used electrospinning set-up.	7
<b>Fig. 2.4</b>	Schematic structures of the employed electrospinning apparatus	9
<b>Fig. 2.5</b>	Instrumental set-up used for dye-doped nanofiber measurements	12
<b>Fig. 2.6.a.</b>	Size distribution results of Ag nanoparticles (a) A sample of silver nanoparticles from the freshly synthesized yellow sol.	13
<b>Fig. 2.6.b.</b>	Size distribution results of Ag nanoparticles (b) A sample from the grayish sol.	14
<b>Fig. 2.7.a.</b>	X-ray diffraction of synthesized silver nanoparticles	15
<b>Fig. 2.7.b.</b>	Ag 3d XPS spectra of Ag nanoparticles on ITO substrates.	15
<b>Fig. 3.1.</b>	SEM photographs of electrospun microfibers and meso porous structures under different	19
<b>Fig. 3.2.I</b>	Signal change of the Ag-free EC based sensing cocktail upon exposure to the oxygen concentrations of a: 0%, b:2, c:5 d:10, e:20, f: 40, g:60–100%.	21
<b>Fig. 3.2.II</b>	Stern Volmer plot derived from quenching based data of the Ag-free EC based sensing cocktail.	22
<b>Fig. 3.3.I</b>	Signal change of the nano-silver containing EC based sensing cocktail upon exposure to the oxygen concentrations of a: 0.2%, b:2, c:5 d:10, e:20, f: 40, g: 60 h: 80 (I) 100% [O <sub>2</sub> ].	22
<b>Fig. 3.3.II</b>	Stern–Volmer plot derived from quenching based data of the Ag NP containing EC based sensing cocktail.	23
<b>Fig. 3.4.I</b>	Lifetime based data of the embedded Ru dye in different matrices upon exposure to certain concentrations of oxygen. Silver doped and silver free EC	24
<b>Fig. 3.4.II</b>	Lifetime based data of the embedded Ru dye in different matrices upon exposure to certain concentrations of oxygen. Silver doped and silver free PMMA.	24
<b>Fig. 3.5.</b>	The UV–Vis absorption spectra of the silver NPs during production.	26
<b>Fig. 3.6.</b>	Emission based kinetic response of mesoporous membranes prepared from EC based matrix after exposure to certain concentrations of O <sub>2</sub> .	27

## ABBREVIATIONS AND SYMBOLS

<b>EC</b>	Ethyl Cellulose
<b>Ag NPs</b>	Silver Nano Particles
<b>Ru(bipy)<sub>3</sub><sup>2+</sup></b>	Tris(2,2'-bipyridyl) ruthenium(II) chloride
<b>TEOS</b>	Trimethoxy silane
<b>ORMOSILs</b>	Organically Modified Silicates
<b>DOP</b>	Dioctyl Phthalate
<b>PMMA</b>	Polymethyl Methacrylate
<b>TCSPC</b>	Time Correlated Single Photon Counting
<b>IRF</b>	Instrument Response Function
<b>SEM</b>	Scanning Electron Microscope
<b>XRD</b>	X Ray Diffraction
<b>NFM</b>	Nanofibrous Membranes
<b>MLCT</b>	Metal-to-Ligand Charge-Transfer
<b>fcc</b>	face centered-cubic
<b>(g)</b>	Gases
<b>&gt;</b>	Bigger
<b>MHz</b>	Mega hertz
<b><math>\chi^2</math></b>	Chi square
<b>eV</b>	Electron Volts
<b>kV</b>	Kilo Volts
<b>I</b>	Luminescence intensities



$k_q$	Quenching constant
$K_{SV}$	Stern–Volmer constant
$\tau$	Decay times of the luminophore
$R^2$	Regression coefficient



## 1. INTRODUCTION

Accurate measurements of oxygen levels are of great importance in environmental and biomedical analysis as well as industrial processes [1]. Today electrochemical and optical sensing strategies have intensively been used for detection of gaseous or dissolved oxygen. The optical chemical sensing approach offers some advantages over electrochemical strategy like shorter response time, easy fabrication, low cost and suitable sensitivity.

Most of the optical oxygen sensors work on the principle of luminescence quenching of different types of organic dyes in oxygen permeable solid matrices. These organic dyes are pyrene and its derivatives [2], pyrene butyric acid, quinoline and phenanthrene [3], transition metal complexes of osmium [4], rhenium [5,6], platinum [7,8], palladium and iridium [9,10], ruthenium [11–17], polypyridine complexes and metalloporphyrins [18].

Covalently assembled monolayer of 61-(p-hydroxy phenyl methano) fullerene molecules has also been used for oxygen sensing [19]. Among these dyes, the ruthenium(II) polypyridine complexes have been the most intensively utilized dye. They produce metal-to-ligand charge transfer excited states which are readily quenched by oxygen. Rochea et al. reported enhanced luminescence for the ruthenium dye in trimethoxysilane (TEOS) xerogel spin-coated on a gold surface.

However, the offered design was highly sensitive only in low O<sub>2</sub> environment [11]. Wu and coworkers investigated the oxygen sensing properties of Ru(II) complexes on mesoporous structures. Approximately 90% of the luminescence of the sensor was quenched upon exposure to 10% of oxygen [14]. In another work, functionalized [Ru(Phen)<sub>3</sub>]<sup>2+</sup> based dyes in mesoporous silica matrix were tested for oxygen sensing purposes.

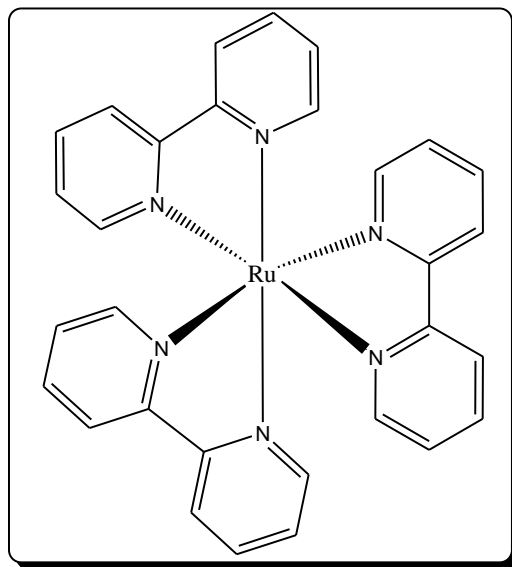


**Fig. 1** Tris(2,2'-bipyridyl)dichlororuthenium(II)

The calibration plots were nonlinear within the measured oxygen concentrations [15]. Not only the ruthenium based dyes but also other transition metal complexes and porphyrin derivatives developed to date exhibit nonlinear calibration data or Stern–Volmer plots especially for the large working ranges [3–18, 20–25]. This is due to the uncontrollable high sensitivity of the exploited dyes towards oxygen. It is obvious that, modeling the calibration related data with linear, quadratic, exponential, and other functions is possible.

However, extrapolation or interpolation of quadratic data requires much more computation power with respect to the linear ones. Such kind of calibration plots and the Stern Volmer plots require some algorithms for linearization.

On the other hand, recently, fabrication of mesoporous, micro and nano-scale matrix materials and their usage for gas sensing purposes have been studied [2,6,7,9,13–17,20–25]. Their porous structure with enhanced surface area, the feasibility of modification and reliable entrapment of fluorescent dyes within the cavities make them useful as solid matrix materials for the design of optical chemical sensors [25]. Besides, the development of micro and nanomaterials will support the design of new sensors, which represent enhanced analytical characteristics such as small size, robustness, low limit of detection values and enhanced relative signal change. To date,

we see that previous work about the sensing of gaseous oxygen with nano or micro-materials are mainly based on the sol gel silica formation or precipitation and micro-emulsion methods for polymers.

The ruthenium complexes were intensively used in silicone [3], sol –gel [26–30], ORMOSILs (organically modified silicates) or in modified ORMOSILs [12,31,32]. A detailed comparison of the performances of such optical oxygen sensors in terms of matrix materials, sensitivity, working range and detection limit has been reported earlier [25]. In the light of the literature information, fabrication of new, transparent, meso or micro-porous materials and nano-scale matrices can be concluded as a promising area in optical chemical sensing of oxygen.

On the other hand it is known that presence of the conducting metallic surfaces like gold and silver is effective on emissive spectral properties of nearby fluorophores. Gryczynski et al. investigated effects of metallic silver particles on the emission properties of  $[\text{Ru}(\text{Phen})_3]^{2+}$  on silver island films [33]. In another recent work influence of metal nanoparticles on fluorescence properties of Ru dye was investigated in solution phase. The samples containing different sizes of silver and gold nanoparticles were titrated with varying concentration of the fluorescent dyes of tris (2,2-bipyridyl) dichloro ruthenium and other fluorophores [34].

These studies encouraged us to investigate effect of silver nanoparticles on oxygen sensing properties of the Ru complex. In this study, we have successfully fabricated nano-silver doped fiber materials and nano-porous film structures of polymers via electrospinning method for sensitive chemical optical detection of  $\text{O}_2(\text{g})$ . By this way, we succeeded to tune the uncontrollable intensive response of the ruthenium dye observed even in low concentrations of oxygen and enlarged the linear working range. As far as we know, this is the first study with silver doped-electrospun fibers and meso-porous polymers on oxygen sensing.

Effects of presence of silver nanoparticles on oxygen sensing were tested and evaluated by steady state and life time based measurements in terms of sensitivity, stability and calibration characteristics.

# **1. INTRODUCTION**

---

## 2. MATERIAL AND METHOD

### 2.1. Materials

All solvents were of analytical grade and purchased from Merck, Fluka, Sigma and Riedel. The O<sub>2</sub> sensitive fluorescent dye, tris(2,2-bipyridyl)ruthenium(II) chloride and plasticizer, dioctyl phthalate (DOP) were supplied from Aldrich. Ethyl cellulose (EC, ethoxy content of 48%) Fig. 2.1 and polymethyl methacrylate (PMMA) Fig. 2.2 were purchased from Organics. The room temperature ionic liquid (RTIL) and 1-butyl-3-methylimidazolium tetrafluoroborate was from Fluka. Silver nitrate (>99% AgNO<sub>3</sub>) and sodium borohydride (99% NaBH<sub>4</sub>) were purchased from Merck and Aldrich Chemical Companies, respectively. Ultra pure water was used in preparation of silver nanoparticles. Glassware was cleaned by soaking in alcoholic KOH. Oxygen and nitrogen gas cylinders were of 99.9% purity and obtained from Gunes Company, Izmir, Turkey.

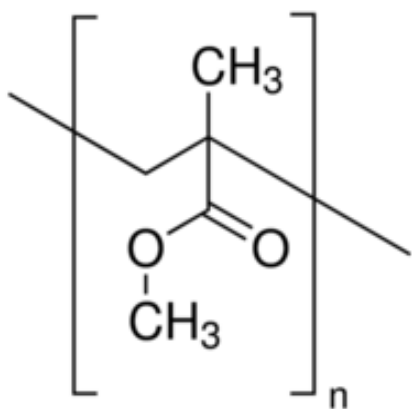


Fig. 2.1 Poly(methyl methacrylate)

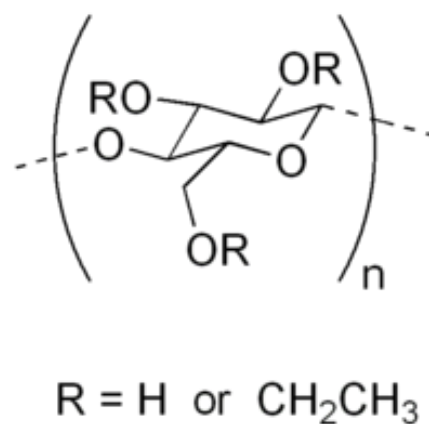


Fig. 2.2 Ethyl Cellulose

### 2.2. Instrumentation

The steady state fluorescence measurements of the sensor films and fibers were recorded by using Varian Cary Eclipse spectrofluorometer. Fluorescence lifetimes were measured by time resolved fluorescence spectrometer of Edinburgh Instruments of FLS

## **2.MATERIAL AND METHOD**

---

920 which works on the principle of time correlated single photon counting (TCSPC) method. The samples were excited with a pico-second pulsed diode laser at the wavelength of 468 nm, at a frequency of 10 MHz. The excitation and emission slits were set to 5 nm. During measurements, the Instrument Response Function (IRF) was obtained from a non-fluorescing suspension of a colloidal silica (LUDOX 30%, Sigma Aldrich) in water, held in 10 mm path length quartz cell and was considered to be wavelength independent. The lifetime parameters were recovered by reiterative convolution (reconvolution) with a weighted, nonlinear least-squares method using the measured IRF and emission decay data. The reduced chi-squared values and plots of weighted residuals were used to determine the ‘goodness of fit’ between the calculated and measured decay curves. In all cases the calculated chi square values ( $\chi^2$ ) were less than 1.2 and the residuals trace symmetrically distributed around the zero axes.

The programmable syringe pump (Top Syringe Pump Top 5300) and the high voltage power supply (Gamma High Voltage ES30) were used for fabrication of electrospun fibers or films. The surface morphology of the fibers and films were studied using scanning electron microscope (SEM) instrument (FEI QUANTA FEG 250). Size distribution analysis of the silver nanoparticles was performed with a Zetasizer instrument in dispersed form in triethanolamine (Malvern Instruments Ltd.) X ray diffraction patterns of the fabricated Ag NPs were determined with XRD instrument from Thermo Scientific. The diffraction patterns were recorded from 30 to 90° at a speed of 2°/min. The XPS analysis of the Ag NPs was performed with Al-K $\alpha$  irradiation of a Thermo-Scientific instrument. The device was calibrated according to gold; 4f<sub>7/2</sub>. A 10<sup>-8</sup> mbar of vacuum was applied and 20 scans from a single point were recorded. Pass energy and energy step size values were reported as 150 eV and 1 eV, respectively.

### **2.2.1. Electrospinning**

#### **2.2.1.1. Theory of Electrospinning**

Electrospinning is a technique used to prepare nanostructured surfaces by electrostatic force. The working principle of electrospinning is based on the use of a high voltage power supply (in the kV range) able to charge a drop of a polymer pending



from the tip of a syringe or pipette, and to overcome its surface tension. When the potential applied between the needles of the syringe (filled with the polymer) and the grounded collector is high enough, the drop of the polymers becomes charged, deformed in a Taylor cone and suddenly ejected.

Charging of the jet occurs at the base, with solutions of higher conductivity being more conducive to jet formation. Electric forces then accelerate and stretch the polymer jet, causing the diameter to decrease as its length increases. Additionally, solvents with high vapor pressures may begin to evaporate, causing a decrease in jet diameter and velocity. During elongation, the fiber is formed and deposited randomly on a grounded collector. As the process occurs, new fibers are accumulated and nonwoven Nanofibrous Membranes (NFM) is formed. [41]

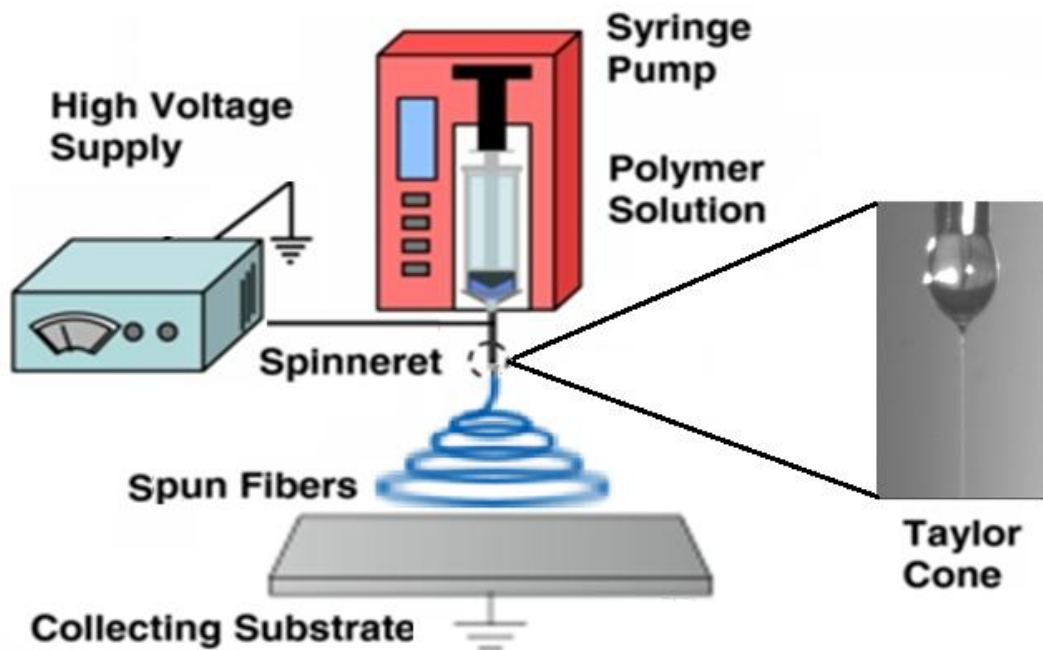


Fig. 2.3 The most frequently used electrospinning set-up.

### 2.2.1.2. Parameters of Electrospinning Process

## **2.MATERIAL AND METHOD**

---

From the previous description of theory, it is clear that the electrospinning process can be manipulated by a number of variables. Doshi and Reneker classified the parameters that control the process in terms of solution properties, controlled variables, and ambient parameters. Solution properties include the viscosity, conductivity, surface tension, polymer molecular weight, dipole moment, and dielectric constant. The effects of the solution properties can be difficult to isolate since varying one parameter can generally affect other solution properties (e.g., changing the conductivity can also change the viscosity). Controlled variables include the flow rate, electric field strength, distance between tip and collector, needle tip design, and collector composition and geometry. Ambient parameters include temperature, humidity, and air velocity. [42]

### **2.2.1.3. Electrospun Nanofibrous Membranes for Sensors Design**

In the recent years, the application of the electrospinning techniques for sensors design is increased. The nanofibers produced through the electrospinning process. This is the case of a nanostructured membrane, where the porous structure allows for an increased accessibility and a low resistance to diffusion to reactive reagents, making these fibers ideal systems as sites for catalysis, nanoreactors, and adsorbents. Because of the higher specific area and electrospun nano materials have applications as sensors and catalysts.

It is expected that this large amount of available surface area has the potential to provide unusually high sensitivity, selectivity, time response, stability, durability, reproducibility, and reversibility are largely influenced by the properties of the sensing materials used. So far, electrospun polymer nanofibers have been investigated as gas sensors, chemical sensors, optical sensors and biosensors. The principle of nanofiber sensors is to utilize the chemical or physical reaction between a targeted material and a sensing material. Furthermore, the sensors convert the result of those chemical or physical phenomena to the optical or electrical output and finally quantitative measurement of the detected materials is conducted.

Electrospun polymer nanofibers used in various sensor applications as gas [43], chemical, optical sensor [44] and biosensors. [45]

#### 2.2.1.4. Electrospinning Apparatus

The homogeneous PMMA or EC solutions were placed in a 10 mL plastic syringe fitted with a metallic needle of 0.4mm of inner diameter. The syringe is fixed vertically on the syringe pump (Top Syringe Pump Top-5300) and the electrode of the high voltage power supply (Gamma High Voltage ES30) was clamped to the metal needle tip. Schematic structure of the electrospinning apparatus is shown in Figure 2.4.

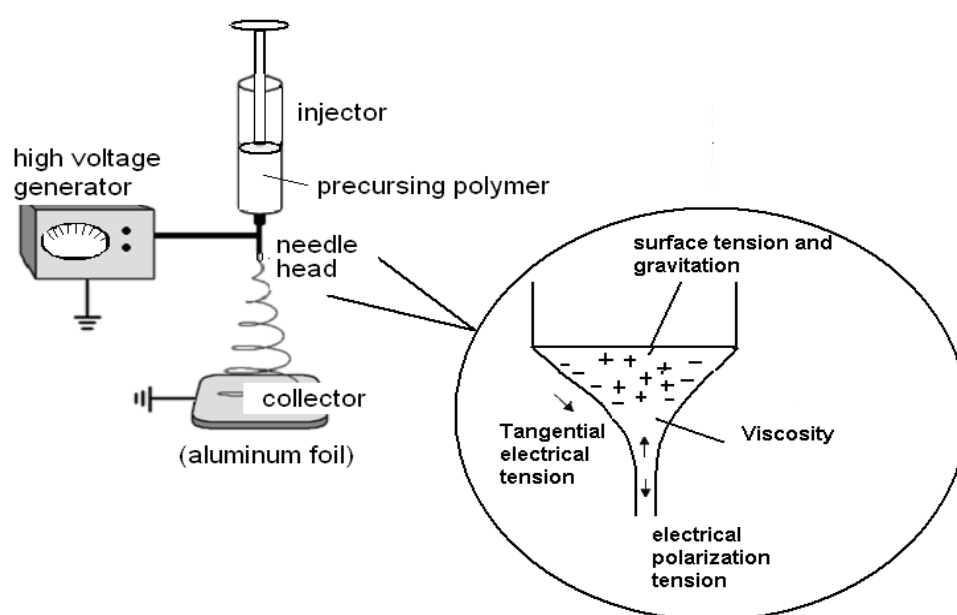


Fig. 2.4 Schematic structures of the employed electrospinning apparatus

#### 2.2.1.5. Principles of Optical Chemical Sensors

Optical chemical sensors which produce an irreversible response are referred to as a 'probe' or 'optode'. It normally consists of the following components:

1. The recognition element, where specific interaction and identification of the analyte take place;
2. The transducer element that converts the recognition process into a measurable

## **2.MATERIAL AND METHOD**

---

optical signal; the optical properties measured can be absorbance, reflectance, luminescence, light polarization, Raman.

3. An optical device (process unit) which consists of at least a light source (in its simplest form a LED);

4. Finally a detector (in its simplest form a photodiode), which detects and converts the change of optical properties, after amplification of the primary signal, into a unit readout. [46]

The optical properties measured can be absorbance, reflectance, luminescence, light polarization, Raman and other.

### **2.2.1.6. Classification of Optical Chemical Sensors**

A chemical sensor is a device that transforms chemical information, ranging from the concentration of a specific sample component to total composition analysis, into an analytically useful signal. A physical sensor is a device that provides information about a physical property of the system. [47]

Optical chemical sensors contain two basic functional units: a receptor part and a transducer part. In the *receptor* part of a sensor the chemical information is transformed into a form of energy which may be measured by the transducer. The *transducer* part is a device capable of transforming the energy carrying the chemical information about the sample into a useful analytical signal.

Optical chemical sensors may be classified according to the operating principle of the transducer.

**1. Optical devices** transform changes of optical phenomena, which are the result of an interaction of the analyte with the receptor part. This group may be further subdividing according to the type of optical properties, which have been exploited in chemical sensors:

a) **Absorbance**, measured in a transparent medium, caused by the absorptivity of the analyte itself or by an indirect reaction with some proper indicator.

b) **Reflectance** is measured in non-transparent moiety, usually using an immobilized indicator.

c) **Luminescence**, based on the measurement of the intensity of light emitted after an excitation or a chemical reaction in the receptor system.

d) **Fluorescence**, measured as the positive emission effect upon exposure to irradiation. Also, selective quenching of fluorescence may be the basis of such devices.

e) **Refractive index**, measured as the result of a change in solution composition. This may include also a surface plasmon resonance effect.

f) **Optothermal effect**, based on a measurement of the thermal effect caused by light absorption.

g) **Light scattering**, based on effects caused by particles of definite size present in the sample.

**2. Electrochemical devices** transform the effect of the electrochemical interaction analyte - electrode into a useful signal.

**3. Electrical devices** based on measurements, where no electrochemical processes take place, but the signal arises from the change of electrical properties caused by the interaction of the analyte.

**4. Mass sensitive devices** transform the mass change at a specially modified surface into a change of a property of the support material.

**5. Magnetic devices** based on the change of paramagnetic properties of a gas being analysed. These are represented by certain types of oxygen monitors.

**6. Thermometric devices** based on the measurement of the heat effects of a specific chemical reaction or adsorption which involve the analyte.

**7. Other physical properties** as for example X-,  $\beta$ - or  $\Gamma$ - radiation may form the basis for a chemical sensor in case they are used for determination of chemical composition.

## 2.MATERIAL AND METHOD

This classification represents one of the possible alternatives. Sensors have also been classified according to the application to detect or determine a given analyte. Examples are sensors for pH, for metal ions or for determining oxygen or other gases. [48]

### 2.3. Gas sensing studies

The gases, O<sub>2</sub> and N<sub>2</sub> were mixed in the concentration range of 0.0–100.0% in a Sonimix 7000 A gas blending system. The out-put flow rate of the gas mixture was maintained at 550 mL min<sup>-1</sup>. Gas mixtures were introduced on the sensing agents via a diffuser needle under ambient conditions. Real time excitation and emission spectra of sensing materials were recorded upon exposure to certain concentrations of oxygen. Instrumental set-up used for dye-doped thin film and nanofiber measurements was shown in Fig. 2.5.

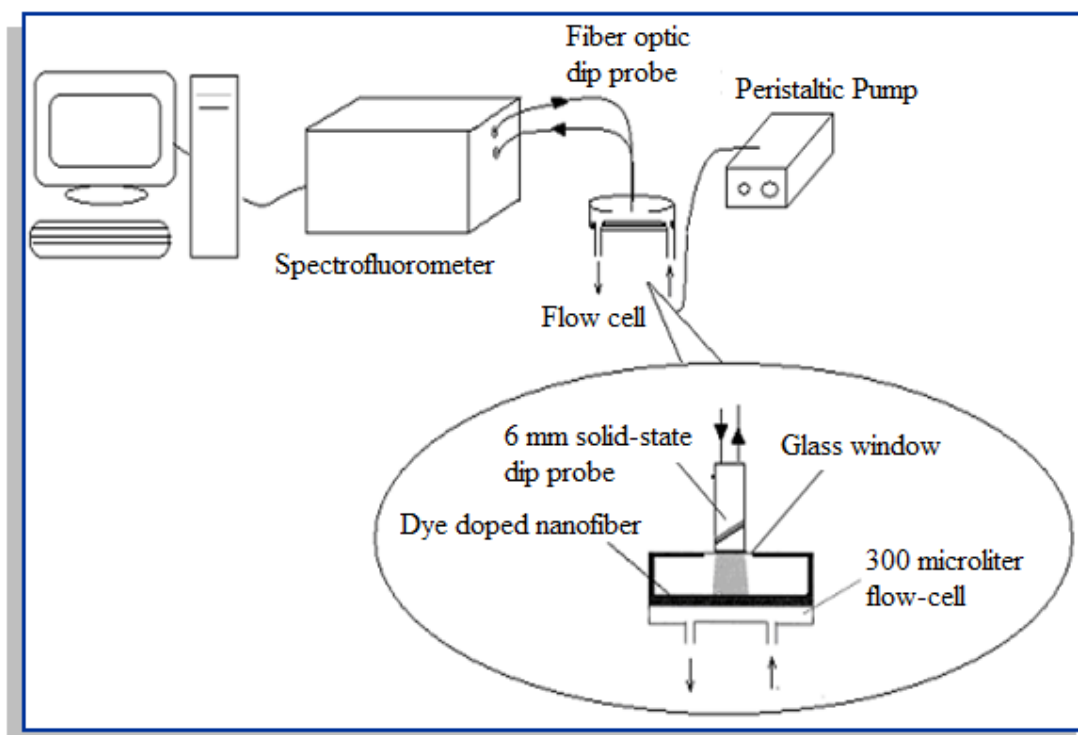


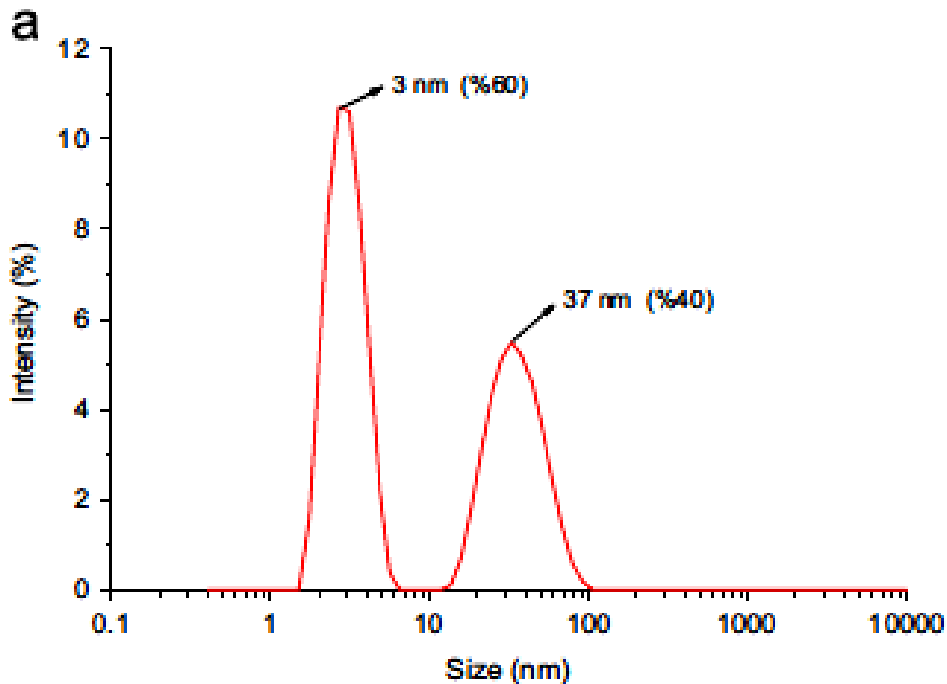
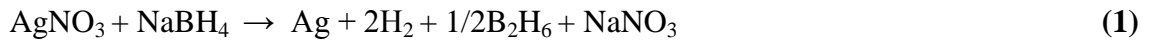
Fig. 2.5 Instrumental set-up used for dye-doped nanofiber measurements

#### 2.4. Preparation of silver nanoparticles

Colloidal silver nanoparticles were synthesized according to the literature method [35] and briefly summarized here. A large excess of sodium borohydride was used to reduce the ionic silver and to keep the silver nanoparticles apart from each other in a coordinated form. A 10 mL volume of 1.0 mM silver nitrate was added dropwise into the 30 mL of 2.0 mM sodium borohydride solution in an ice bath under magnetic stirring. Color of the colloidal solution turned pale yellow after the addition of 2 mL of silver nitrate and following purple and finally gray color when all of the silver nitrate had been added. Later the water content of the sol was evaporated under vacuum and dried silver nanoparticles dispersed in triethanolamine for size distribution analysis.

Zetasizer instrument derived size distribution results of diluted Ag nanoparticles have been shown in Fig. 2.6.

Here the basic chemical reaction is given in Eq. (1) and shows the reduction of silver by sodium borohydride:



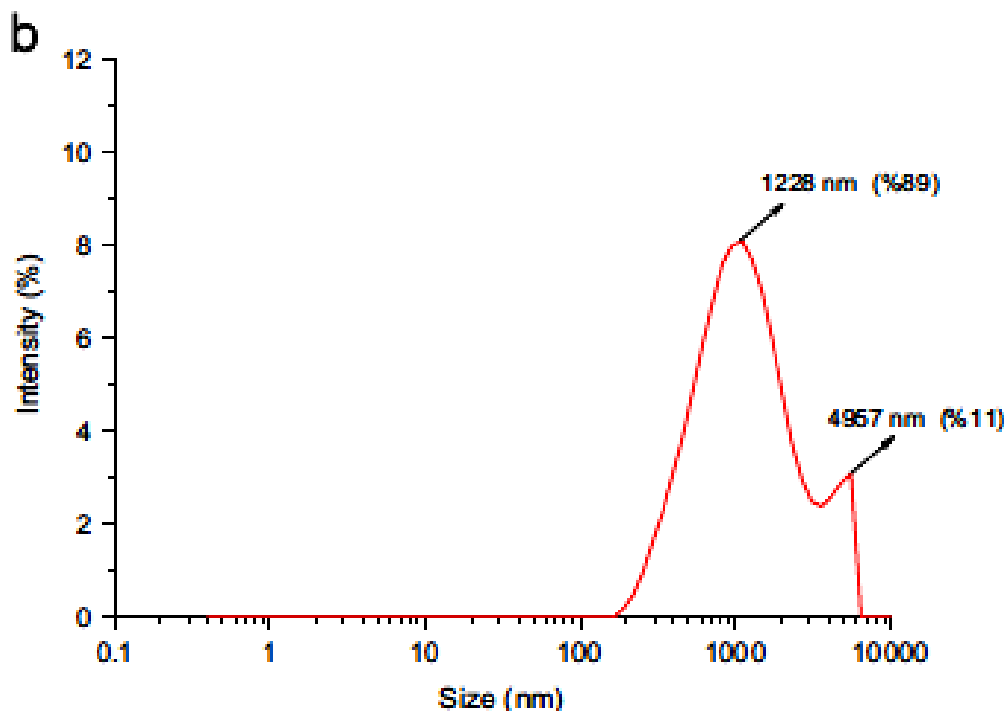


**Fig. 2.6.** Size distribution results of Ag nanoparticles (a) A sample of silver nanoparticles from the freshly synthesized yellow sol. (b) A sample from the grayish sol. (For interpretation of the references to color in this figure legend, the reader is referred to the web version of this article.)

The specific color of the colloidal silver solution is due to the plasmon absorbance. Incident light creates oscillations in conduction electrons on the surface of the silver nanoparticles and electromagnetic radiation is absorbed. The wavelength of the plasmon absorption maximum of the silver nanoparticles in solvent moiety can be used to estimate the particle size [36].

Here the plasmon resonance of the produced metallic silver (in yellow sol) yielded an absorption peak near 400 nm which corresponds to the particle size of 50–70 nm [36].

Under stirring conditions, once all of the silver nitrate has been added, aggregation begins as the yellow sol first turns a darker yellow, then violet and eventually grayish, after which the colloid breaks down and particles settle out. Results of size distribution analysis of the grayish sol have been shown in Fig. 2.6. b

Phase composition and crystallinity characteristics of the synthesized Ag NPs



were investigated by using X-ray diffractometer (see Fig. 2.7. a). The X-ray diffraction patterns correspond to silver with a crystalline face centered-cubic (fcc) structure without any impurity.

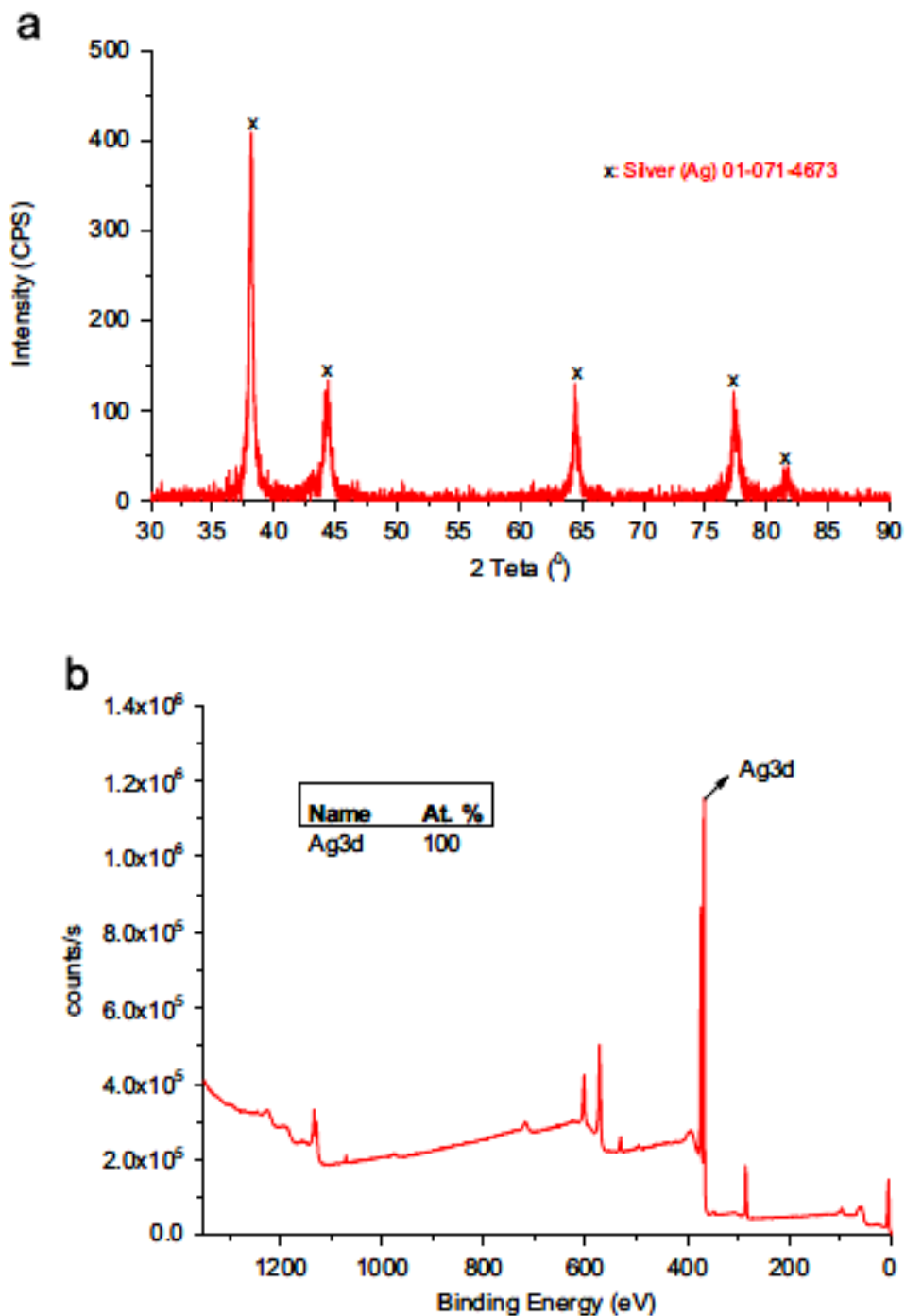


**Fig. 2.7.** (a) X-ray diffraction of synthesized silver nanoparticles (b) Ag 3d XPS spectra of Ag nanoparticles on ITO substrates.

## **2.MATERIAL AND METHOD**

---

In order to determine the chemical environment as well as the oxidation state of Ag NPs, we have performed XPS measurement at the Ag 3d core levels. The Ag 3d<sub>5/2</sub> core level binding energy for Ag NPs appeared at 367.57 which is in good agreement with binding energy of bulk metallic silver [37].

### **2.5. Preparation of electrospun nanofibers**

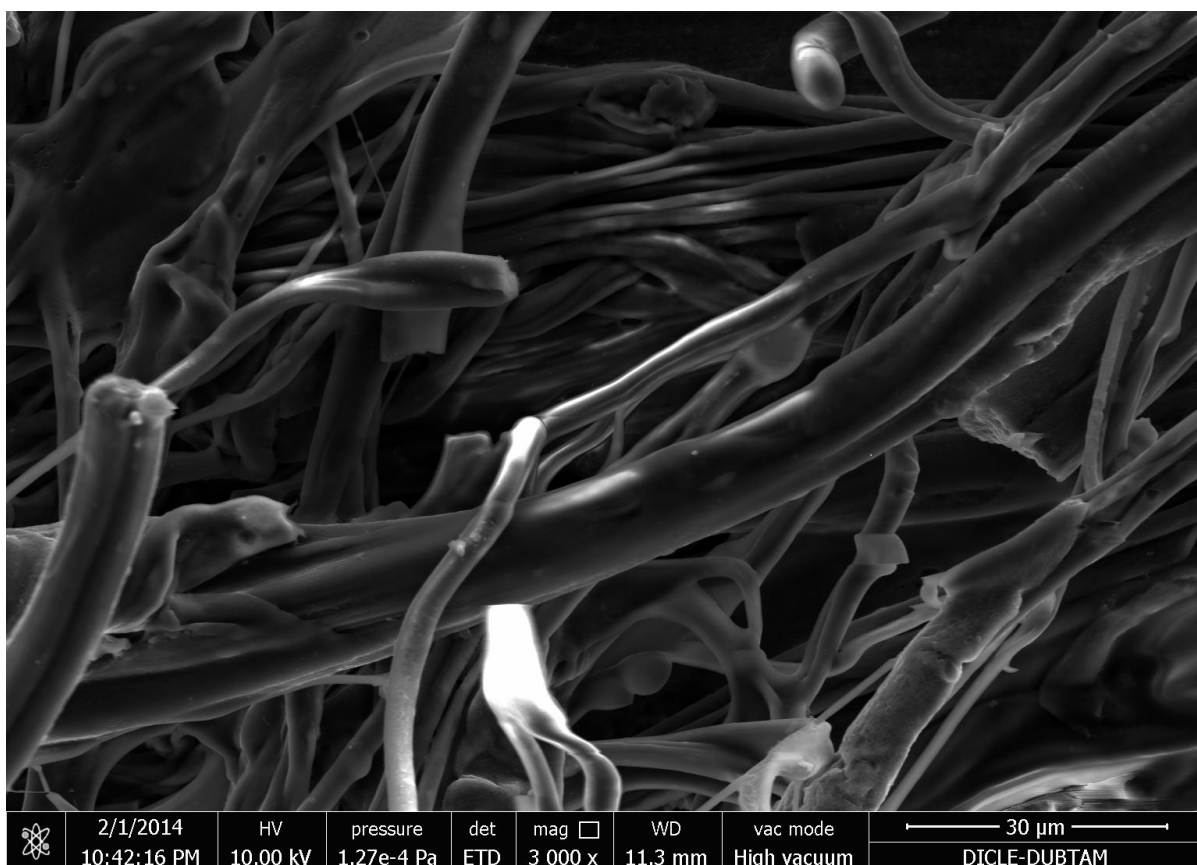
The programmable syringe pump (Top Syringe Pump Top 5300) and the high voltage power supply (Gamma High Voltage ES30) were used to fabricate electrospun fibers. In this process, sensing composites were prepared exploiting two different types of neutral polymers; ethyl cellulose (EC) and polymethyl methacrylate (PMMA). The resulting composites were prepared by mixing 240 mg of polymer, 192 mg of plasticizer (DOP), 5 mg of Ru dye, 48 mg of IL and 1.0 mg of metallic nano-silver, in CH<sub>2</sub>Cl<sub>2</sub>: EtOH (v/v, 1:3). For the preparation of fibers, electrospinning was used as a fast and simple method. The homogeneous polymer solutions were placed in a 10 mL plastic syringe fitted with a metallic needle of 0.4 mm of inner diameter. The syringe was fixed vertically on the syringe pump and the electrode of the high voltage power supply was clamped to the metal needle tip. The feed rate of polymer solution was 1.0 mL/h, the applied voltage was 25 kV and the tip-to-collector distance was 10 cm. The electrospinning process was performed in a dust free closed glass cabin at 20.0 °C. Upon exposure to sufficiently high voltage, the electrical forces act in opposition to and overcame the surface tension of the fluid and a stream of polymer jet was produced. The solvent evaporated and very fine fibers or porous structures were completely coated on the clean aluminum foil.

### 3. RESULTS AND DISCUSSION

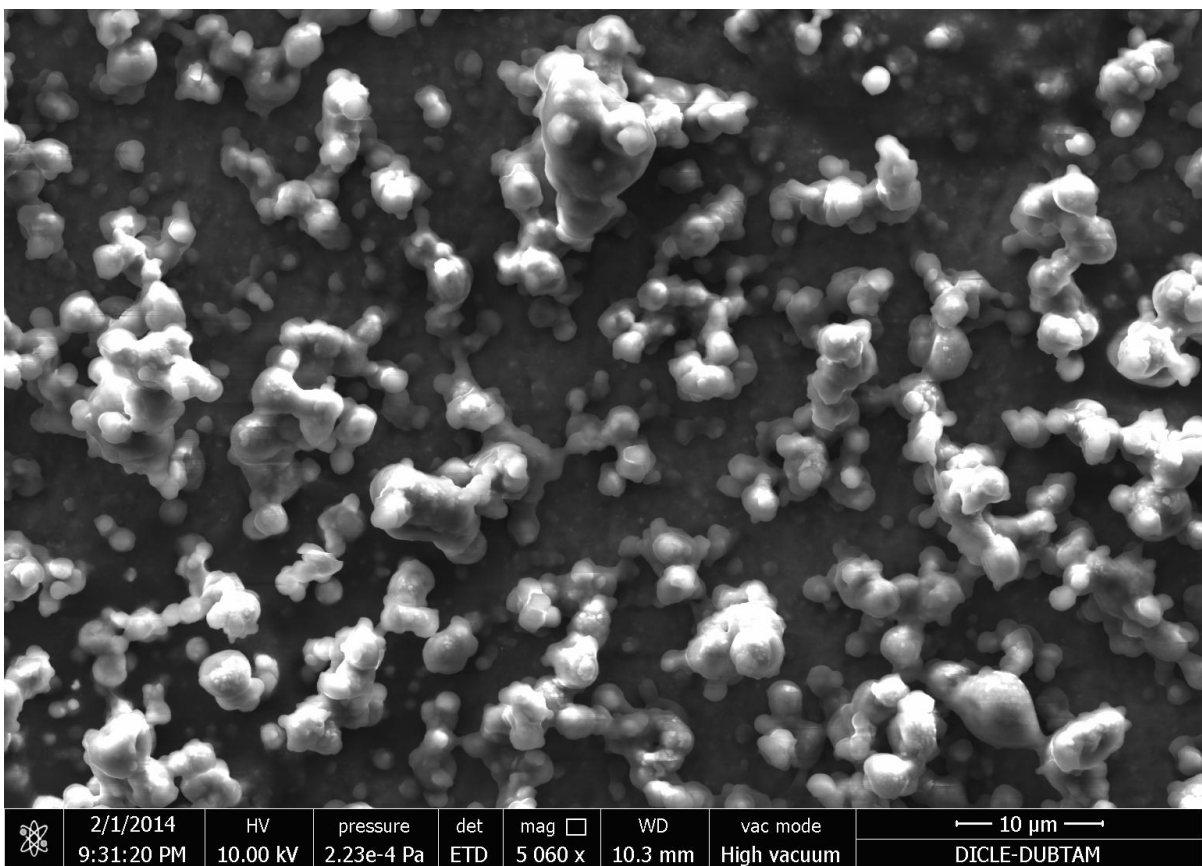
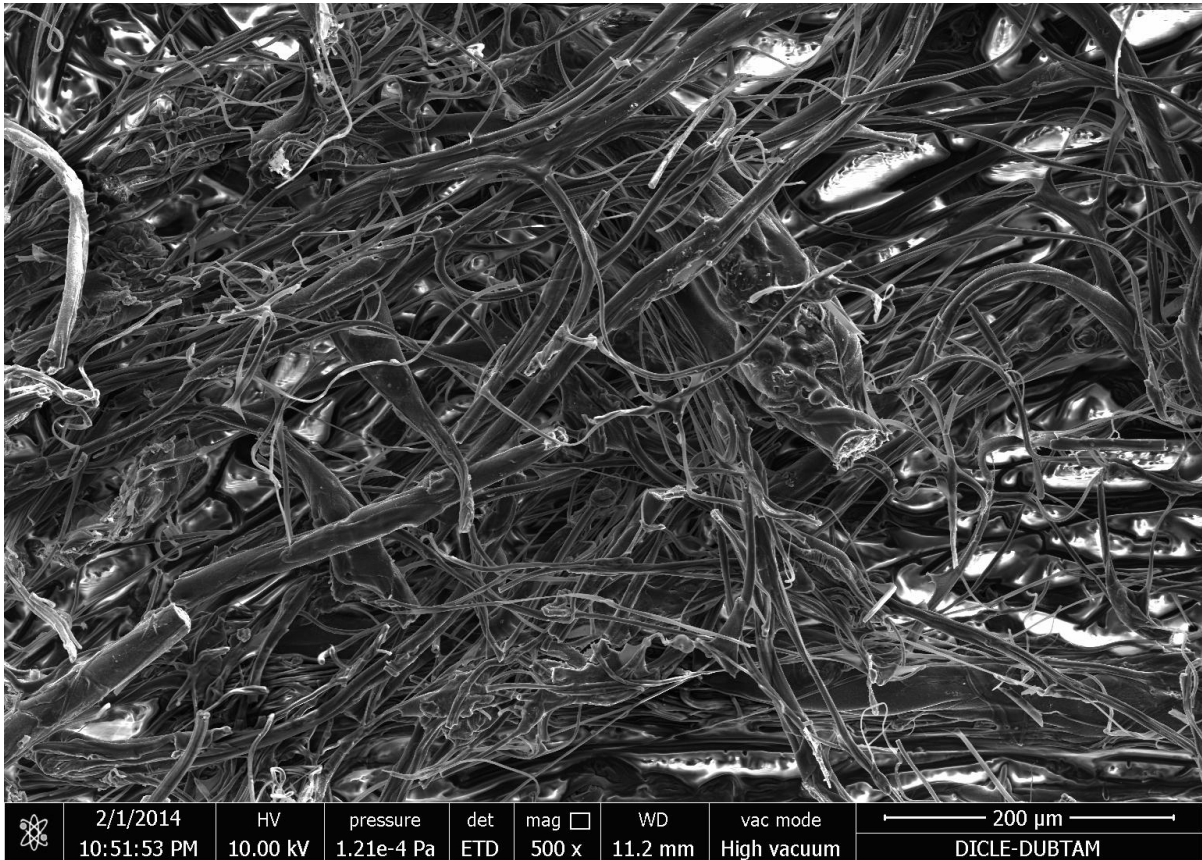
#### 3.1. Structural aspect of the sensing materials

In this work, we exploited the ruthenium complex ( $\text{Ru}(\text{bipy})_3^{2+}$ ) together with Ag NPs in form of, microfibers and porous surfaces. By this way, we compared structures of silver free and silver containing compositions.

We produced the fibers and porous surfaces by exploiting the simple electrospinning technique and characterized them with SEM photographs. While, the EC based cocktails resulting with a porous structure, the PMMA based ones were in fiber forms. The scanning electron microscope (SEM) images of electrospun membranes of different compositions at various magnifications were shown in Fig. 3.1.



### 3. RESULTS AND DISCUSSION



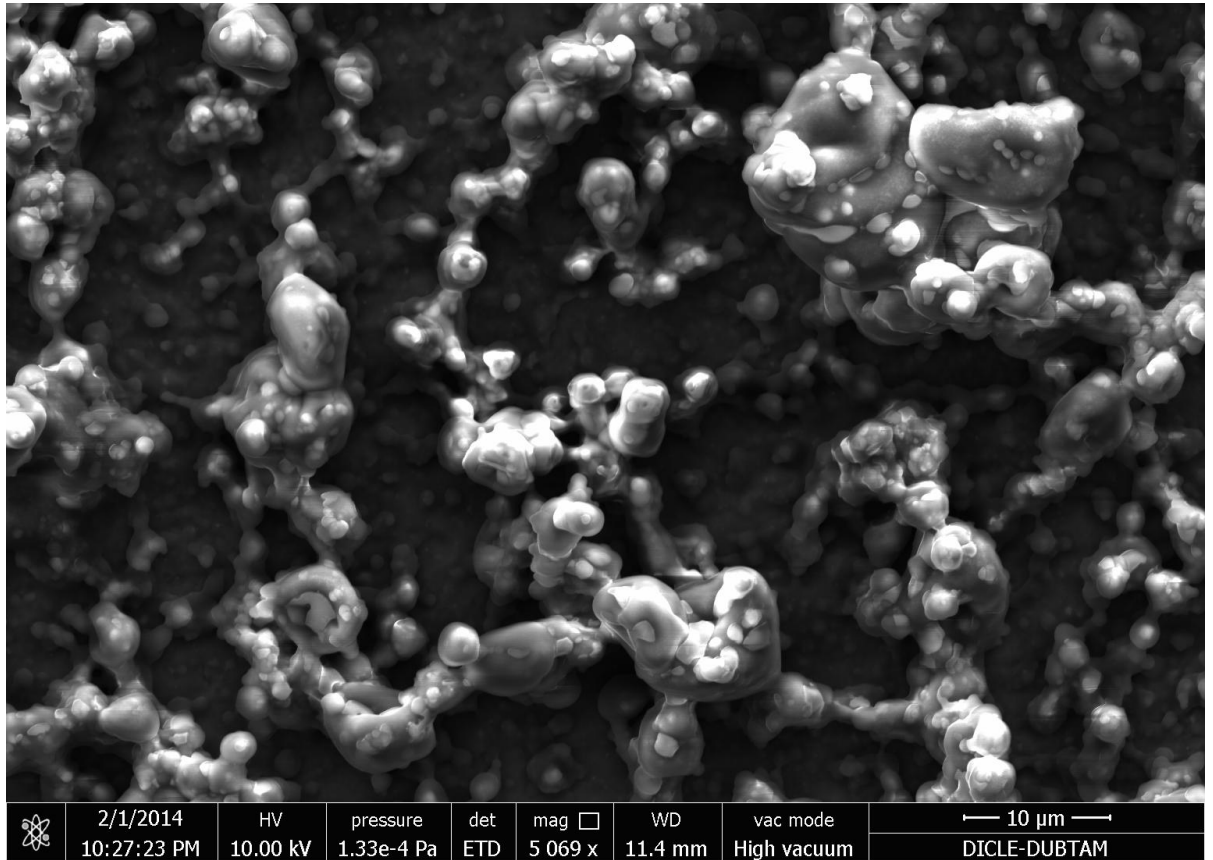


**Fig. 3.1.** SEM photographs of electrospun microfibers and meso porous structures under different magnifications.

In both cases, the empty spaces of the holes within the network structures allow satisfactory diffusion of  $O_2$ . It was observed that the electrospun membranes made up of PMMA exhibited 3D network like structure with a random fiber orientation that was evenly distributed on the substrate. The diameters of the fibers varied between 10 nm and 640 nm. This type of fibrous-structure of the electrospun membrane provides higher surface area than that of continuous thin films. Production of nanofibers and further increase of the surface area may be achieved by changing conditions of the electrospinning process such as solvent composition, viscosity, concentration, temperature, humidity and working distance, which results in either smaller diameter fibers or increased porosity at the fiber surface [38].

### 3.2. Fluorescence based measurements

We acquired oxygen induced fluorescence intensity, lifetime and kinetic based data following the signal of the ruthenium dye in the polymeric matrix, in presence and

### 3. RESULTS AND DISCUSSION

---

absence of silver NPs. The acquired data were evaluated for fibrous and porous forms of materials. We utilized the RTIL in all of the matrices in the ratio of 25%. As reported earlier the imidazolium based ionic liquid acts in two different ways in sensing composites. Presence of the positively charged imidazolium and negatively charged tetrafluoroborate ions in the matrix provides enough electrical conductivity under high voltage for the spinning process. Second benefit of the ionic liquid is the enhancement of the oxygen solubility within the matrix due to the presence of fluorine in form of  $\text{BF}_4^-$ . We have also observed that the presence of Ag NPs facilitated the electrospinning process by increasing the electrical conductivity.

#### 3.3. Oxygen sensing studies

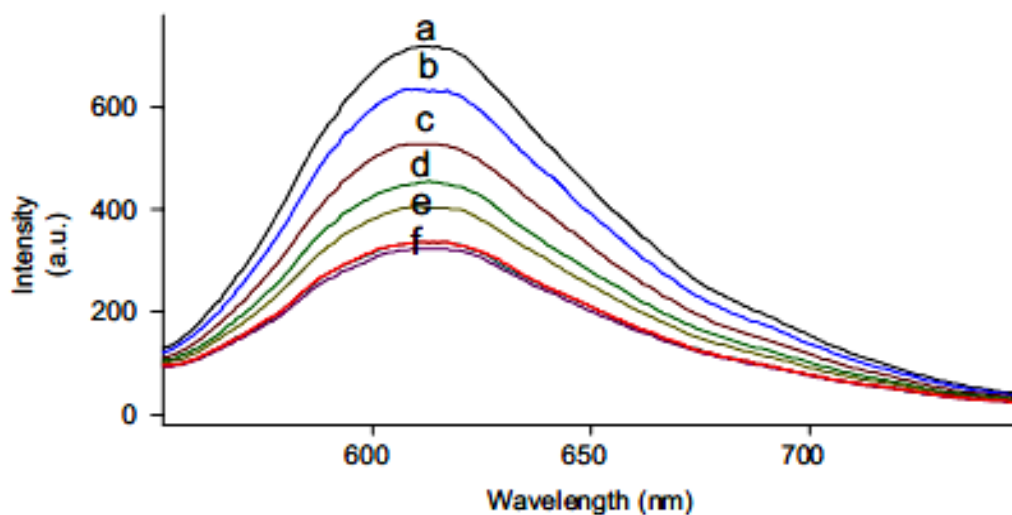
Upon excitation at 460 nm, the employed ruthenium complex yielded emission around 610 nm both in EC and PMMA based matrices. Therefore, the quenching of the excited state luminescence intensity of the luminophore by oxygen molecules was monitored at 610 nm. Triplet oxygen is able to quench efficiently the fluorescence of ruthenium complex via collisions with the fluorophore in its excited state leading to a non-radiative energy transfer. This effect is called “dynamic fluorescence quenching”. The degree of quenching relates to the frequency of collisions, and therefore to the concentration, pressure, temperature and matrix material of the sensor. If the luminescence quenching is purely dynamic, both the intensity and excited state lifetimes are related to the oxygen concentration by the Stern–Volmer equation: where  $I_0$  and  $I$  are the luminescence intensities and  $\tau_0$  and  $\tau$  are decay times of the luminophore in the absence and presence of oxygen, respectively.  $K_{SV}$  is the Stern–Volmer constant,  $[\text{O}_2]$  is the oxygen concentration and  $kq$  is the quenching constant, which is related to the diffusion coefficient of oxygen throughout the matrix. For an ideal homogeneous environment, a plot of the ratio of  $I_0/I$  or  $\tau_0/\tau$  versus  $[\text{O}_2]$  yields a straight line with an intercept at 1 and a slope of  $K_{SV}$ , which is a measure of sensor sensitivity.

$$I_0 / I = \tau_0 / \tau = 1 + K_{SV}[\text{O}_2] = 1 + kq\tau_0[\text{O}_2] \quad (2)$$

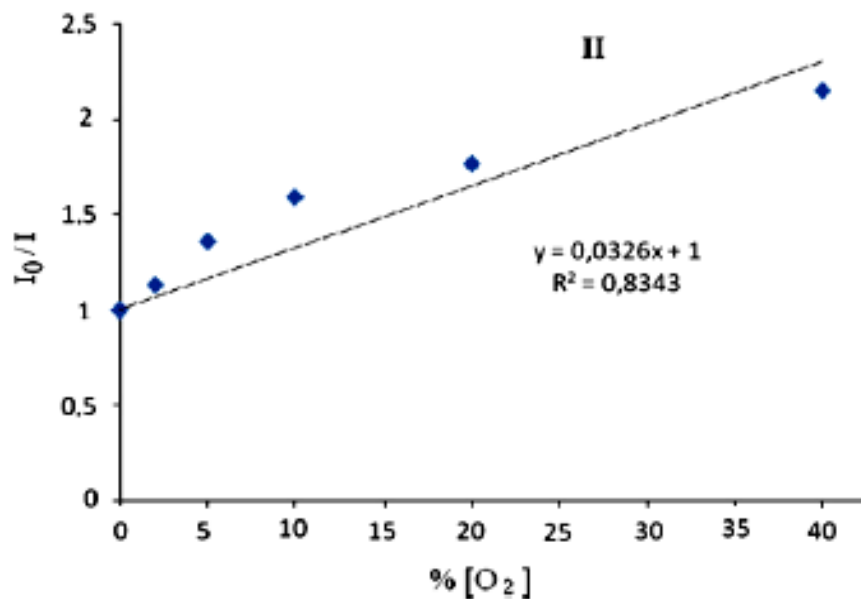
If the luminophore is distributed in heterogeneous sites in the solid matrix, the

Stern–Volmer plot becomes nonlinear. Most of the optical oxygen sensors developed to date exhibited such nonlinear Stern–Volmer plots [34,35]. In this work, the intensity based oxygen induced Stern–Volmer plots of  $\text{Ru}(\text{bpy})_3^{2+}$  were produced for Ag-free and Ag containing matrices for oxygen concentrations in the range of 0.0 – 100.0%. The  $K_{SV}$  values extracted from the slopes of the plots were found to be 0.03 and 0.01 for two moieties, respectively.

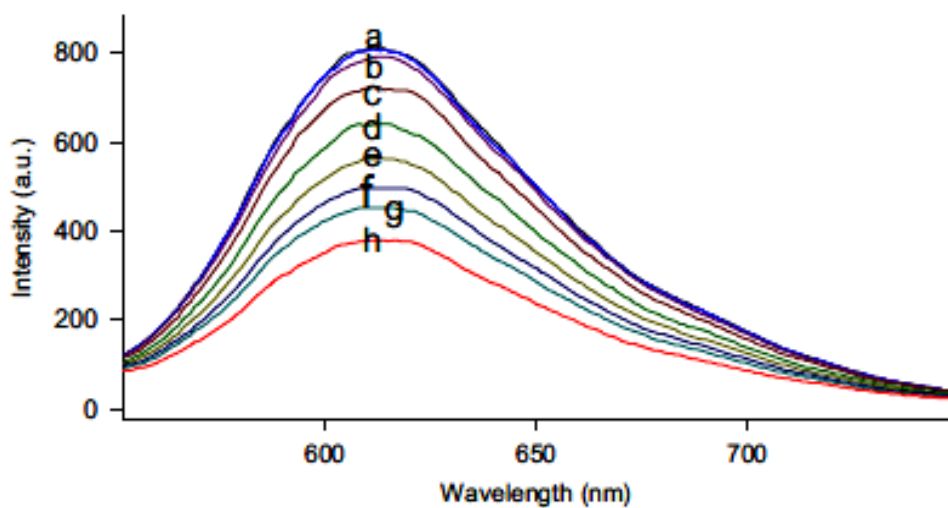
In accordance with literature information, the Ag-free matrices yielded typical non-linear intensity based Stern–Volmer plots ( $R^2=0.8343$ , Fig. 3.2. I and II). However, the plots derived from the silver containing matrices were considerably linear with a regression coefficient of  $R^2=0.9956$  (Fig. 3.3 I and II). This enhancement in linearity in calibration plots can be attributed to the presence of the silver nanoparticles within the sensing matrix.



### 3. RESULTS AND DISCUSSION



**Fig. 3.2.** (I) Signal change of the Ag-free EC based sensing cocktail upon exposure to the oxygen concentrations of a: 0%, b:2, c:5 d:10, e:20, f: 40, g:60–100%. (II) Stern Volmer plot derived from quenching based data of the Ag-free EC based sensing cocktail.





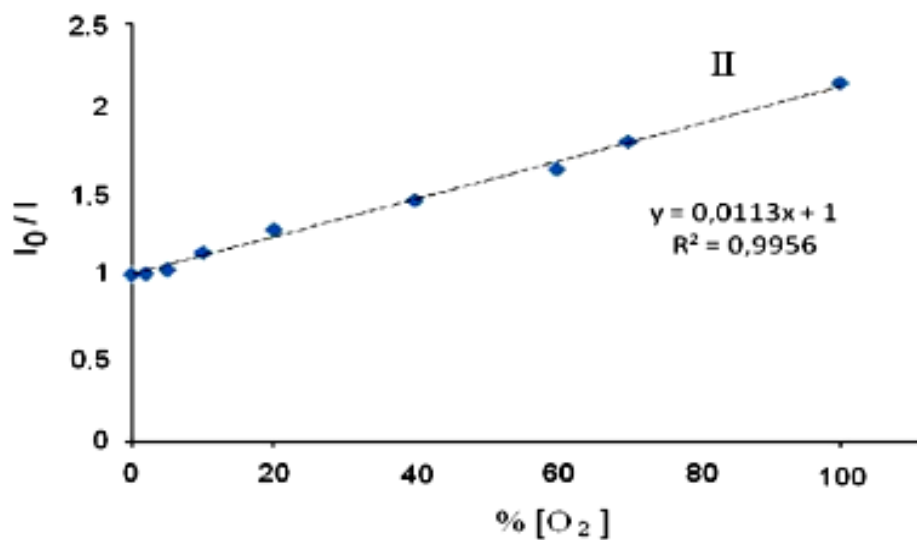


**Fig. 3.3.** (I) Signal change of the nano-silver containing EC based sensing cocktail upon exposure to the oxygen concentrations of a: 0<sub>2</sub>%, b:2, c:5 d:10, e:20, f: 40, g: 60 h: 80 (II) 100% [O<sub>2</sub>]. (II) Stern–Volmer plot derived from quenching based data of the Ag NP containing EC based sensing cocktail.

In order to clarify effect of the Ag NPs on the quenching characteristics we also investigated lifetime based data of the  $[Ru(Phen)_3]^{2+}$  dye both in presence and absence of the metallic silver. The dye exhibited increased decay times both in PMMA and EC matrices when doped together with silver NPs with respect to the Ag-free ones. However, upon exposure to oxygen the decay times decreased in all moieties. Fig. 3.4 I and II shows oxygen induced decay times of the employed sensing agents in a comparative manner. In both matrices, slopes of the decay plots are higher in silver doped moieties.

### 3. RESULTS AND DISCUSSION

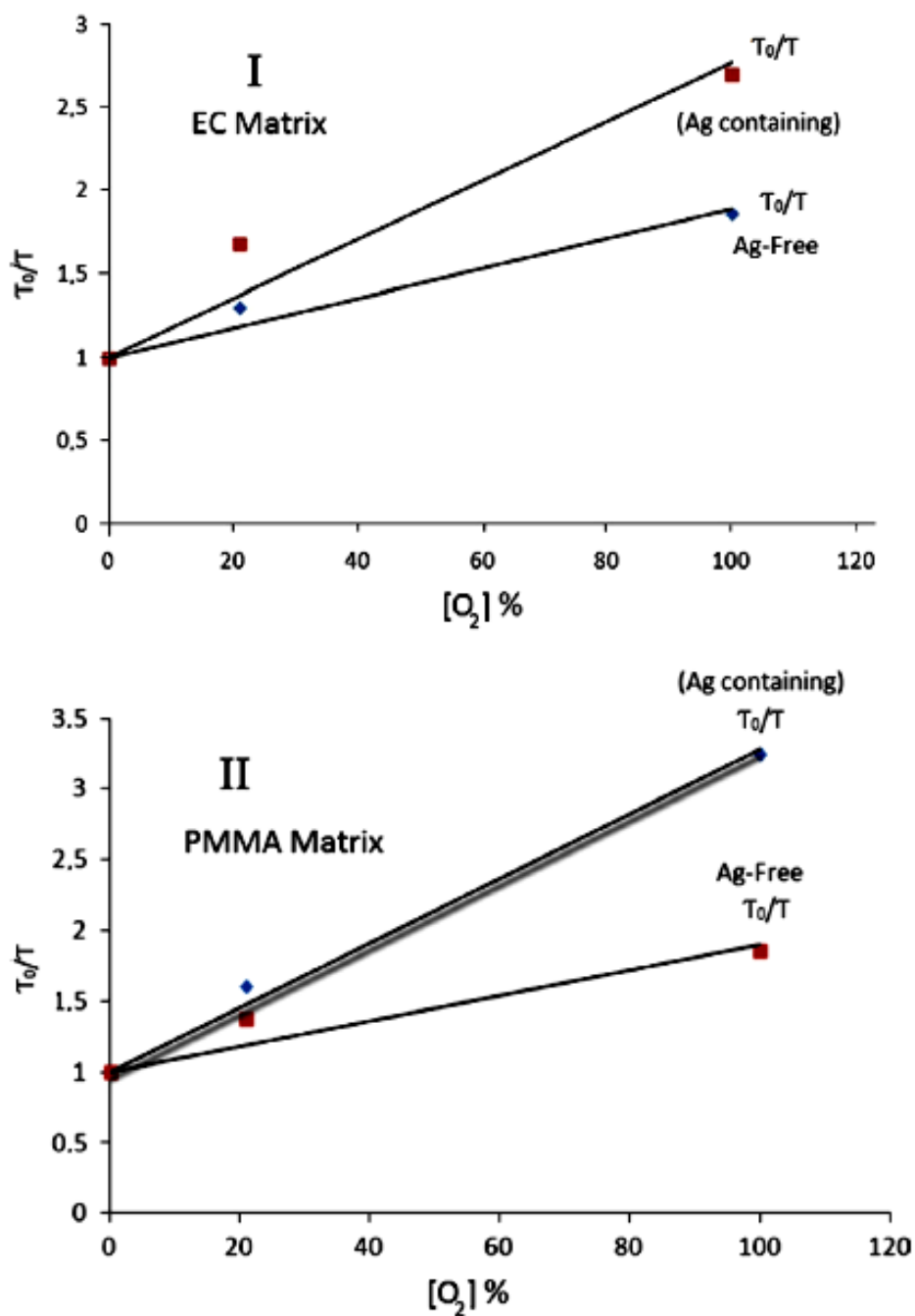


**Fig. 3.4.** Lifetime based data of the embedded Ru dye in different matrices upon exposure to certain concentrations of oxygen. (I) silver doped and silver free- EC, (II) silver doped and silver free PMMA.

When intensity based data (Stern–Volmer plots) and lifetime measurements were evaluated together, will be informative in the explanation of the mechanism of the quenching. In all of the employed matrices, both, the intensity-based and the lifetime based data affected from the increasing oxygen concentrations in direction of decrease. This result can be concluded as the evidence of the dynamic quenching for all moieties.

The slop of quenching plot shown in Fig. 3.2. II (which looks like enhancement due to the algorithm  $I_0/I$ ) is quite sharp for the concentration range of 0.0–20.0% [O<sub>2</sub>]. Additionally, the linear working range is limited between 0.0 and 10.0% [O<sub>2</sub>]. However in case of nano-silver doped films, characteristics of the calibration plot are totally different. The calibration plot becomes linear for the concentration range of 0.0–100.0% [O<sub>2</sub>]. The observed linearity in the oxygen response of the Ru dye should separately be explained on basis of spectral consequences also considering absorption characteristics of the doped silver NPs.

For this reason we recorded absorption characteristics of the silver NPs at different stages of the particle formation (see Fig. 3.5). In the beginning, no absorption peaks were observed for the diluted sols (Fig. 3.5a). With the increase in silver content in sol, and, an accompanying enlargement in diameters of NPs, the characteristic plasmon absorbance peaks of metallic nano-silver appeared at 400–415 nm (Fig. 3.5, lines b and c).

The intensities of the peaks increased and their position gradually shifted from 400 to 450 nm and finally to 550 nm with the increase of diameters of the silver NPs. The possible reason for the red shifts is likely to have been the formation of the larger size particles and the broadened size distribution (ranging from 10 to 535 nm), and even, the non-spherical shapes of silver nanoparticles, which has been mentioned in previous reports [39,40].

### 3. RESULTS AND DISCUSSION

---

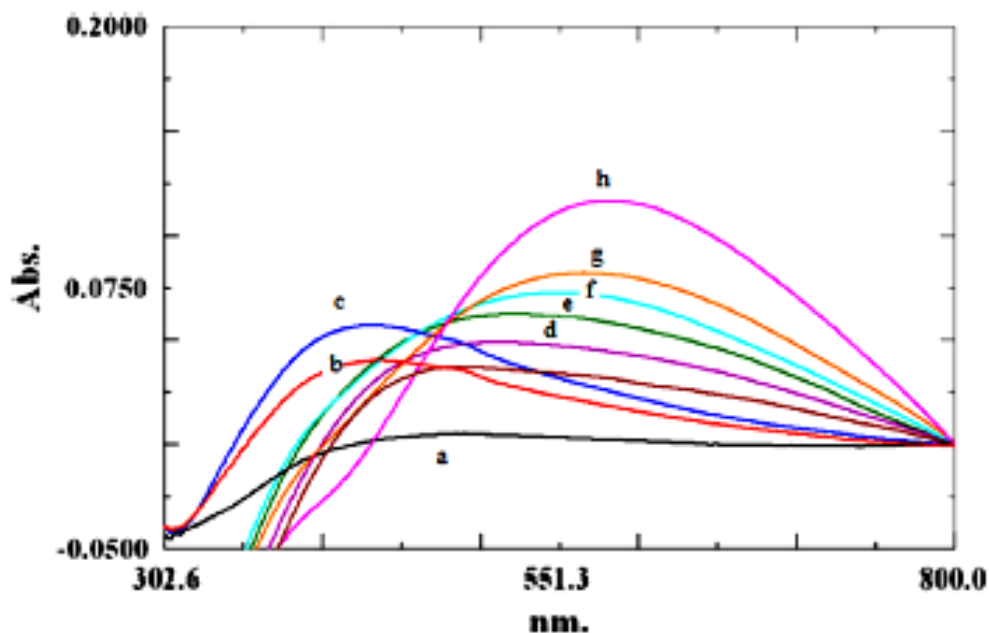


Fig. 3.5. The UV-Vis absorption spectra of the silver NPs during production.

On the other hand,  $\text{Ru}(\text{bpy})_3^{2+}$  dye, undergoes a metal-to-ligand charge-transfer (MLCT) electronic transition in the visible range around 450 and 650 nm. The 610 nm emission band of  $\text{Ru}(\text{bpy})_3^{2+}$  which overlaps with the plasmon absorption of Ag nanoparticles.

Therefore the 610 nm emission of  $\text{Ru}(\text{bpy})_3^{2+}$  may be absorbed by the AgNPs located in close proximity within the same matrix resulting with an energy transfer. This energy transfer from donor  $\text{Ru}(\text{bpy})_3^{2+}$  to acceptor AgNPs is also dependent on the amount of the doped metallic silver. If one utilizes optimized amount of the metallic silver (3.8 m mol AgI/kg polymer), the quenching based oxygen response of the  $\text{Ru}(\text{bpy})_3^{2+}$  becomes tuned.

However, in presence of excess amount of silver, the oxygen response of the Ruthenium dye disappears. Therefore, presence of the silver NPs within the matrix, tunes the sharp and quadratic response of the  $\text{Ru}(\text{bpy})_3^{2+}$  for the small concentrations of gaseous oxygen.

### 3.3.1. Response time and regeneration related sensor dynamics

Response and regeneration performances were presented for Ag-free and Ag-containing matrices. Fig. 3.6 illustrates the response characteristics of EC based sensing materials in an alternating atmosphere of O<sub>2</sub> and N<sub>2</sub>, respectively.

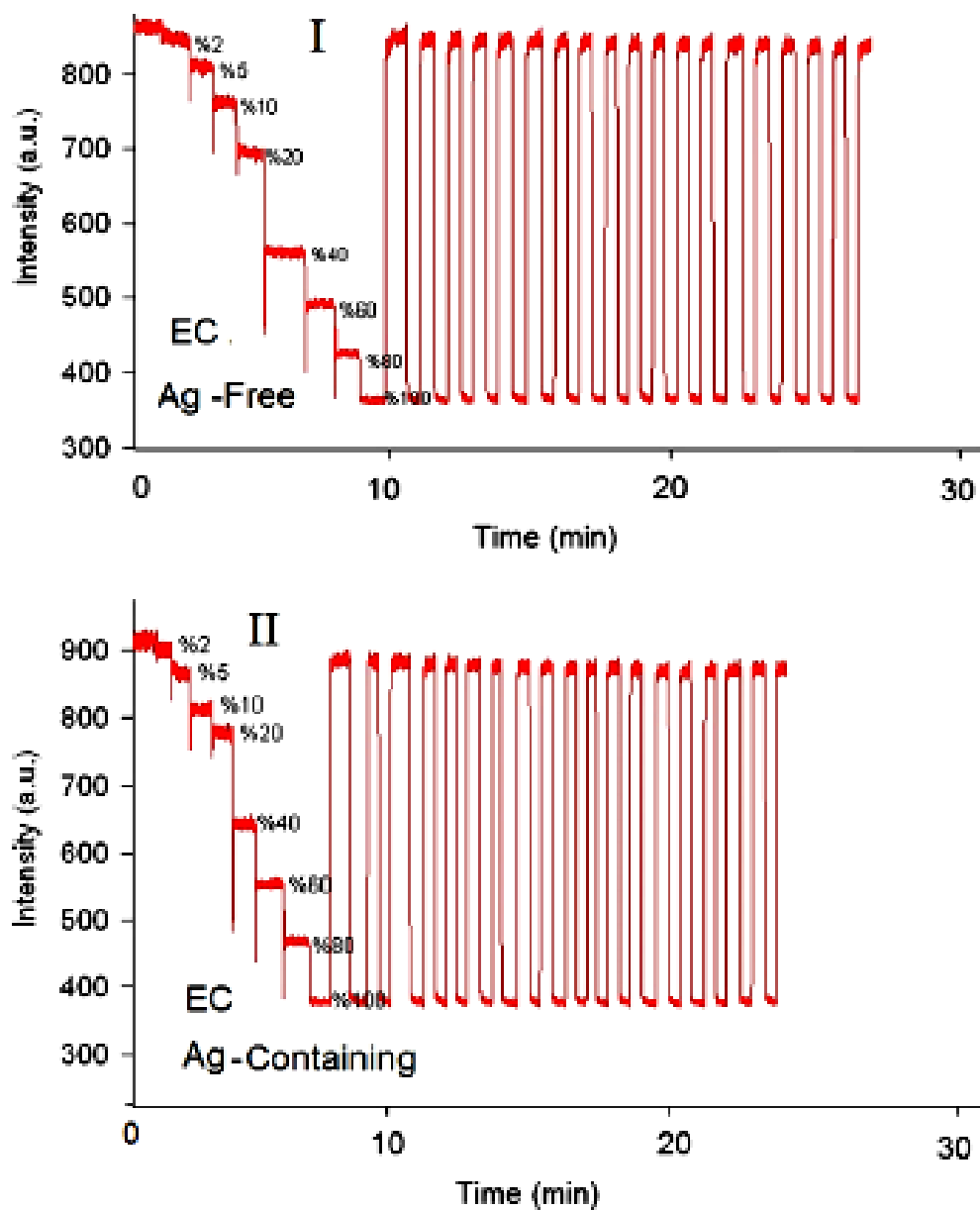


**Fig. 3.6.** Emission based kinetic response of mesoporous membranes prepared from EC based matrix after exposure to certain concentrations of O<sub>2</sub>.

### **3. RESULTS AND DISCUSSION**

---

Response time is defined as the time taken to attain 90% of the signal intensity ( $\tau_{90}$ ) when the gas is changed. In this work four of the sensing composites were tested during 20 cycles. For EC based sensing materials, Ag-free and Ag containing composites completed the cycles in 27 and 24 min, respectively. The individual response times of Ag-free forms were in the range of 3–19 s when going to higher O<sub>2</sub> concentrations. Both for the EC and PMMA based matrices, the silver-doped composites exhibited shorter response times with respect to the Ag-free forms.

For two cases shown in Fig. 3.6, after exposure to 100 and 0% O<sub>2</sub> for 20 replicate measurements, relative standard deviation of upper and lower signal levels were less than 4%. We have demonstrated that, the nano-silver doped sensor fibers and mesoporous slides exhibited a stable and reproducible response for oxygen measurements for a large concentration range.

#### **4. CONCLUSION**

In this work, we used fluorescent ruthenium dye in EC and PMMA based plasticized matrices together with silver nanoparticles for detection of oxygen. Electrospinning was used as to fabricate the sensor slides. The utilization of nano-silver Nanosilver doped slides exhibited a tuned sensitivity and larger linear dynamic working range for the oxygen than that of Ag-free ones made up of same material.

The utilization of nano-silver particles also facilitates the electrospinning process by increasing the electrical conductivity. Additionally, the offered composites provided extraordinary long term stability more than 1 year. Our long term stability tests are still in progress. The long lasting stability of  $\text{Ru}(\text{bpy})_3^{2+}$  can be attributed to the stable oxidation state of the silver and the dye within the employed matrix. Additionally, the immobilized Ag-nanoparticles can provide other benefits like antibacterial effect which can lead medical applications.

#### **4. CONCLUSION**

---



**5. REFERENCES**

- [1] X.D. Wang, O.S. Wolfbeis, *Anal. Chem.* 85 (2013) 487.
- [2] Y. Fujiwara, Y. Amao, *Sens. Actuators, B* 89 (2003) 58.
- [3] T. Ishiji, M. Kaneko, *Analyst* 120 (1995) 1633.
- [4] W.Y. Xu, K.A. Kneas, J.N. Demas, B.A. DeGraff, *Anal. Chem.* 68 (1996) 2605.
- [5] L. Sacksteder, J.N. Demas, B.A. DeGraff, *Anal. Chem.* 65 (1993) 3480.
- [6] T. Hirao, S. Fukuhara, *J. Org. Chem* 63 (1998) 7534.
- [7] P.J. Cywinski, A.J. Moro, S.E. Stanca, C. Biskup, G.J. Mohr, *Sens. Actuators, B* 135 (2009) 472.
- [8] W. Wu, W. Wu, S. Ji, H. Guo, P. Song, K. Han, L. Chi, J. Shaoa, J. Zhao, *J. Mater. Chem.* 20 (2010) 9775.
- [9] S.M. Borisov, T. Mayr, G. Mistlberger, K. Waich, K. Koren, P. Chojnacki, I. Klimant, *Talanta* 79 (2009) 1322.
- [10] M. Marin-Suarezdel Toroa, J.F. Fernandez-Sancheza, E. Baranoff, Md K. Nazeeruddinb, M. Graetzel, A. Fernandez-Gutierrez, *Talanta* 82 (2010) 620.
- [11] P.J.R. Rochea, M.C.K. Cheunga, K.Y. Yungb, A.G. Kirka, V.P. Chodavarpua, F. V Bright, *Sens. Actuators, B* 147 (2010) 581.
- [12] J. Estella, D. Wencel, J.P. Mooreb, M. Sourdain, C. McDonagh, *Anal. Chim. Acta* 666 (2010) 83.
- [13] F. Lupo, M.E. Fragala', T. Gupta, A. Mamo, A. Aureliano, M. Bettinelli, A. Speghini, A. Gulino, *J. Phys. Chem. C* 114 (2010) 13459.
- [14] X. Wu, L. Song, B. Li, Y. Liu, *J. Lumin.* 130 (2010) 374.
- [15] H. Zhang, B. Lei, W. Mai, Y. Liua, *Sens. Actuators, B* 160 (2011) 677.
- [16] B. Wang, Y. Liuc, B. Li, S. Yue, W. Li, *J. Lumin.* 128 (2008) 341.
- [17] H. Zhang, B. Li, B. Lei, W. Li, *J. Lumin.* 128 (2008) 1331.
- [18] A. Gulino, S. Giuffrida, P. Mineo, M. Purrazzo, E. Scamporrino, G. Ventimiglia, M.E. van der Boom, I. Fragala, *J. Phys. Chem. B* 110 (2006) 16781.

## 5. REFERENCES

---

- [19] A. Gulino, S. Bazzano, G.G. Condorelli, S. Giuffrida, P. Mineo, C. Satriano, E. Scamporrino, G. Ventimiglia, D. Vitalini, I. Fragala, *Chem. Mater.* 17 (2005) 1079.
- [20] A. Fercher, S.M. Borisov, A.V. Zhdanov, I. Klimant, D.B. Papkovsky, *ACS Nano* 5 (2011) 5499.
- [21] X-H. Wang, H-S. Peng, H. Ding, F-T. You, S-H. Huang, F. Teng, B. Dong, H.W. Song, *J. Mater. Chem.* 22 (2012) 16066.
- [22] X-H. Wang, H-S. Peng, Z. Chang, L-L. Hou, F-T. You, F. Teng, H-W. Song, B. Dong, *Microchim. Acta* 178 (2012) 147.
- [23] M.R. Chatni, D.E. Maier, D.M. Porterfield, *Sens. Actuators, B* 141 (2009) 471.
- [24] C-S. Chu, Y-L. Lo, *Sens. Actuators, B* 151 (2010) 83.
- [25] M.Z. Ongun, O. Oter, G. Sabancı, K. Ertekin, E. Celik, *Sens. Actuators, B* 183 (2013) 11.
- [26] C. McDonagh, P. Bowe, K. Mongey, B.D. MacCraith, *J. Non-Cryst. Solids* 306 (2002) 138.
- [27] C. McDonagh, B.D. MacCraith, A.K. McEvoy, *Anal. Chem.* 70 (1998) 45.
- [28] H. Zhang, B. Li, B. Lei, W. Li, S. Lu, *Sens. Actuators, B* 123 (2007) 508.
- [29] Tang Z. Tao, R.M. Bukowski, E. h C. Tehan, S. Karri, A.H. Titus, F.V. Bright, *Analyst* 131 (2006) 1129.
- [30] O. Oter, K. Ertekin, S. Derinkuyu, *Mater. Chem. Phys.* 113 (2009) 322.
- [31] C-S. Chua, Y-L. Lob, *Sens. Actuators, B* 155 (2011) 53.
- [32] Y. Xiong, D. Zhu, S. Chen, H. Peng, Y. Guan, *J Fluorescence* 20 (2010) 269.
- [33] I. Gryczynski, J. Malicka, E. Holder, N. Dicesare, J.R. Lakowicz, *Chem Phys Lett.* 372 (2003) 409.
- [34] V. K. Kandimalla, Influence of metal nanoparticles on fluorescence properties, Master's Theses and Doctoral Dissertations, 2010 Paper 371.
- [35] P.C. Lee, D. Meisel, *J. Phys. Chem.* 86 (1982) 3391.

- [36] S.D. Solomon, M. Bahadory, A.V. Jeyarajasingam, S.A. Rutkowsky, C. Boritz, J. Chem. Educ. 84 (2007) 322.
- [37] J. Moghimi-Rad, T.D. Isfahani, I. Hadi, S. Ghalamdaran, J. Sabbaghzadeh, M. Sharif, Appl. Nanosci. 1 (2011) 27.
- [38] J.M. Deitzel, J. Kleinmeyer, N.C. Tan, Polymer 42 (2001) 261.
- [39] X. Ye, Y. Zhou, J. Chen, Y. Sun, Appl. Surf. Sci. 253 (2007) 6264.
- [40] A. Zielinska, E. Skwarek, A. Zaleska, M. Gazda, J. Hupka, Procedia Chem 1 (2009) 156
- [41] Matteo Scampicchio,\*a Andrea Bulbarello,b Alessandra Arcchi,b M. Stella Cosio,b Simona Benedetti,b Saverio Mannino
- [42] Electrospinning of polymeric nanofibers for tissue engineering applications: a review quynh p. pham,\* upma sharma, ph.d.,\* and antonios g. mikos, ph.d.
- [43] Ding, Wang, Yu & Sun, 2009
- [44] Wang, Drew, Lee, Senecal, Kumar & Samuelson, 2002
- [45] Scampicchio, Bulbarello, Arcchi, Cosio, Benedetti & Mannino, 2012; Manesh, Santhosh, Gopalan & Lee
- [46] The Development of Ionophore-Selective Based Optical Chemical Sensors for the Determination of Heavy Metal Ions in Aqueous Environments Li Li, MSc. (Hons)
- [47] Hulanicki, Geab, & Ingman, 1991
- [48] Hulanicki, Geab, & Ingman, 1991

## **5. REFERENCES**

---

## **RESUME**

---

### **RESUME**

**Name and Surname** : OSMAN ÖZTÜRK

**Place of Birth** : AMASYA

**Date Of Birth** : 12.12.1979

**Marital Status** : MARRIED

**Foreign Language** : ENGLISH AND GERMAN

**Educational Status (Institutions and Year) :**

**High School** : SULUOVA HIGH SCHOOL/1993-1996

**Undergraduate** : ANADOLU UNIVERSITY/1998-2005

**Master** : DİCLE UNIVERSITY/2011-2014

**Working Institution** : TURKISH ARMED FORCES